Atmospheric Rivers and Weather Types in Aotearoa New Zealand: a two-way story

— Supplementary Materials —

Benjamin Pohl[1]*; Hamish D. Prince[2]; Jonathan Wille[3]; Daniel G. Kingston[4]; Nicolas J. Cullen[4]; Nicolas Fauchereau[5]

[1] Biogéosciences, UMR6282 CNRS / Université de Bourgogne Franche-Comté, Dijon, France
[2] Department of Atmospheric and Oceanic Sciences, University of Wisconsin-Madison, Madison, WI, USA
[3] Université Grenoble Alpes/CNRS/IRD/G-INP, IGE, Grenoble, France
[4] School of Geography, University of Otago, Dunedin, New Zealand
[5] National Institute of Water and Atmospheric Research, Auckland, New Zealand

In these Supplementary Materials, we present figures that could not appear in the main paper to keep it concise. They could yet be useful to some readers.

Supplementary Figure 1 shows AR counts for each grid-point of Fig. 1b, when all AR events are retained after applying the detection algorithm of Guan and Waliser (2019). Results differ from those presented in the main paper, which consist in removing those events that do not come from the open sea. This is especially true for the eastern parts of ANZ, where angle-based filtering removes most of the events coming from the west and that cross the topographic barrier of the Southern Alps.

Supplementary Figure 2 replicates the results of Fig. 4 but for the 10% strongest AR events, as measured by their associated vertically-integrated moisture transport. Although the predominant roles of the main types (T or, for some regions, W) remain qualitatively unchanged, some non-negligible differences can be found for some of the regions of ANZ. Concerning the ERA5 redefinition of the types, some examples involve type HNW for the southeastern regions (grid-points #0, #1 and #3; see Fig. 1b for their location), and, surprisingly, for the east coast of the North Island (#11), or TNW for the central-eastern parts of ANZ (#7, #9, #11). This suggests that particularly strong AR events may result (i) from differences in specific humidity in the air mass, especially for the northern parts of ANZ, as discussed in the main text and below, but also (ii) from potentially different synoptic-scale south of ANZ, with an increasing contribution of the types that chanel the moisture fluxes from the west or southwest towards the southern coasts of ANZ.

Supplementary Figure 3 shows composite precipitation anomalies during the main WTs associated with ARs, when they do vs. do not co-occur with AR events. For overall WT

occurrences, this analysis resembles previous studies that explored the relationships between WTs and daily precipitation amounts and anomalies (e.g., Renwick 2011). However, closer scrutiny reveals different statistical significance as compared to previous work. Large parts of the territory show non-significant anomalies at the 95% (e.g., west of ANZ during occurrences of type T), while this type was considered as a synoptic configuration yielding wet conditions west of the main divide. These apparent contradictions are mostly due to the nonparametric Welch test used here, more appropriate to non-Gaussian variables than the more commonly used parametric t-test. The fact that some anomalies do not reach statistical significance (Fig. 5), in spite of large departures from the average climatology, suggests large within-type diversity, when all days ascribed to a given WT are considered. Indeed, daily precipitation anomalies associated with the same WTs specifically for NoAR days (that is, WT occurrence not accompanied by any AR occurrence), show anomaly fields that more often reach the 95% significance bound. This further confirms that AR occurrence, concomitantly with WTs, is a key parameter to consider to explain the internal variability of the latter, as discussed in the main paper. Comparing Supp. Fig. 3a (analyzing AR events that reach the south of ANZ) and 3b (considering those events that hit the north of the country) also shows that some common WTs recurrently involved in AR development in both regions (e.g., types T or SW) further differentiate during AR days, depending on their landfalling regions. While AR presence or absence is a first major cause of within-type diversity, second-order differentiation is also due to the location and shape of those ARs, with respect to ANZ.
These results are fully confirmed, and are graphically more visible, in Supp. Figs. 4 and 5, based on the rank of daily precipitation anomalies during overall WT occurrences, and then, separating NoAR and AR days. Although they are more intense, daily precipitation during AR events also appear more concentrated, spatially, which seems coherent with the narrow moisture corridors that are formed by these events.

Supplementary Figure 6 replicates the results of Fig. 7 for the AR events that landfall over the south and the north of ANZ. These results are in line with those discussed in the main article, and confirm that synoptic configurations, as approximated here by their discretization into 12 WTs, have a major influence on AR angles (and therefore on the zonal and meridional components of their corresponding IVT). Weaker (but still significant) influence is also found for AR duration and time-integrated total moisture transport, the latter being mostly determined by the former.
The AR filtering based on their angle, as shown in Supp. Fig. 1, is more restrictive for grid-point #0 than #16 (which is more surrounded by sea, hence a larger proportion of ARs that are retained in the analysis). This has a strong incidence on the statistical distribution of AR properties in grid-point #0.

Supplementary Figure 7 similarly generalizes the results of Fig. 8 for the north and south of ANZ, by assessing how regional atmospheric circulation differs between AR and NoAR days, during each favorable WT. The major conclusions are the same as those outlined in the main paper for the West Coast of the South Island: during AR days the atmospheric centers of action are shifted to form a geopotential height dipole that acts to chanel moisture fluxes towards the region of interest (that is, the landfalling region of the corresponding AR events).
Depending on the landfalling region of the ARs, the geopotential dipole that is strengthened during those events shows different locations and orientations. In the main article, we identified (Fig. 8) a negative geopotential pole southwest of ANZ, and a positive one north to northeast of it, which directed northwesterly atmospheric fluxes towards the landfalling West Coast

region of the South Island, perpendicularly to the coast and topographic barrier (Fig. 1). Although the general mechanisms and conclusions are verified for all landfalling regions along the coasts of ANZ, the dipole pattern varies in location and angle from one landfalling region to another, which is further informative to identify possible moisture sources and moisture corridors (Bennett and Kingson 2022):
— for the south of ANZ (Supp. Fig. 7), a meridional dipole prevail, with a negative pole south of ANZ and a positive pole most frequently located over Tasman Sea. This acts to reinforce the dominant westerly winds, thereby increasing their moisture transport. The positive pole west of ANZ favors an anticyclonic circulation that could favor northerly anomalies from Australia towards the mid-latitudes and that could increase the humidity of the air mass, through poleward moisture export.
— for the northern regions of ANZ (Supp. Fig. 8), the negative pole of geopotential height is found immediately to the west of ANZ, while the positive pole is located northeast of the North Island. This dipole is favorable to northerly or northwesterly anomalies that could direct moisture fluxes, potentially originating from the Tasman or Coral seas, towards the north of ANZ. Such moisture transport could be very efficient, if the air mass contains much moisture.

This question of the humidity of the air mass is explored in Supp. Fig. 9. Here, lower-layer moisture fluxes are shown, together with anomalies of specific humidity at 1000hPa, during overall WT occurrences. Next we analyze the within-type diversity, by calculating the differences between NoAR and moderate AR days on the one side, and strong minus moderate AR days on the other side. These analyses are performed for both the West Coast region of South Island (Supp. Fig. 9a), extensively discussed in the main paper, as well as the southernmost (Supp. Fig. 9b) and northernmost (Supp. Fig. 9c) landfalling grid-points of ANZ. Results first identify the major role of meridional anomalies in driving moisture anomalies, southerly winds being associated with an advection of cold, dry air towards the lower latitudes while the reverse prevails with northerly anomalies (Supp. Fig. 9).
Under AR conditions, the air mass is significantly more humid than during NoAR days associated with the same WT. The causality between dynamics and thermodynamics remains to be established, as the main moisture sources feeding AR events with moisture. Our results depict increasing importance of air humidity towards the north of ANZ, while moisture transport reaching the southern part of the country seem more related to the modulus of mid-latitude westerly winds.

Finally, Supplementary Figure 10 explores day-to-day variability in AR properties, within a given synoptic context (that is, WT), and their relationships with these synoptic-scale configurations around ANZ. They confirm the results discussed in the main article for the West Coast region of the South Island, as well as the synoptic differences identified in Supp. Figs. 7-9 between AR and NoAR days associated with the same WT.

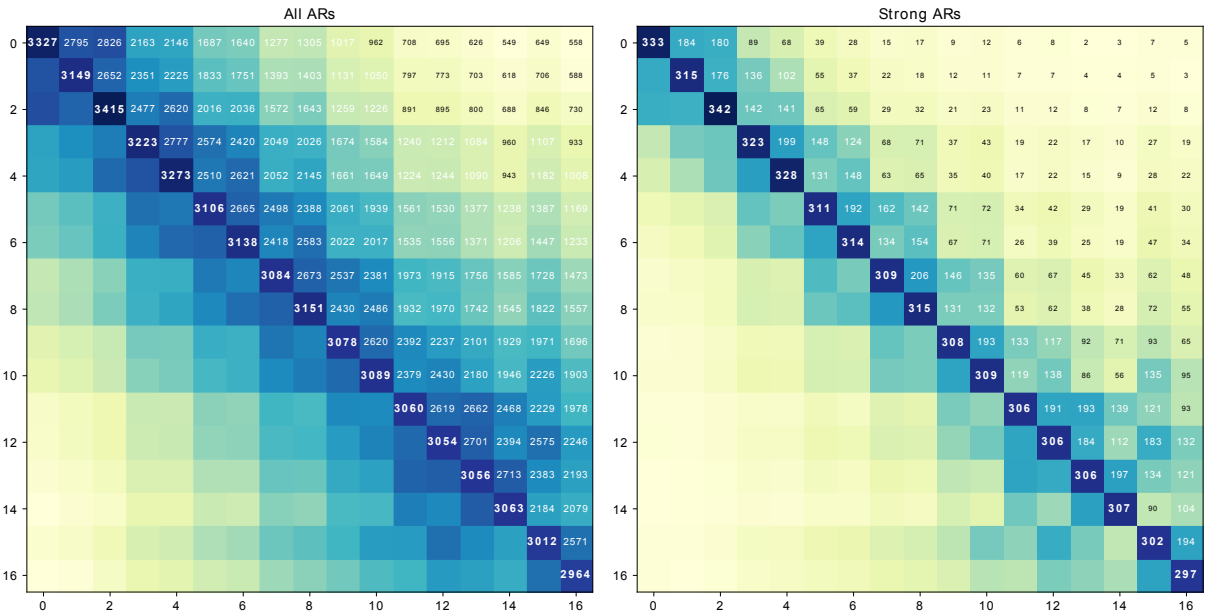

Supplementary Figure 1. As Fig. 3 but without removing AR events based on their angle.

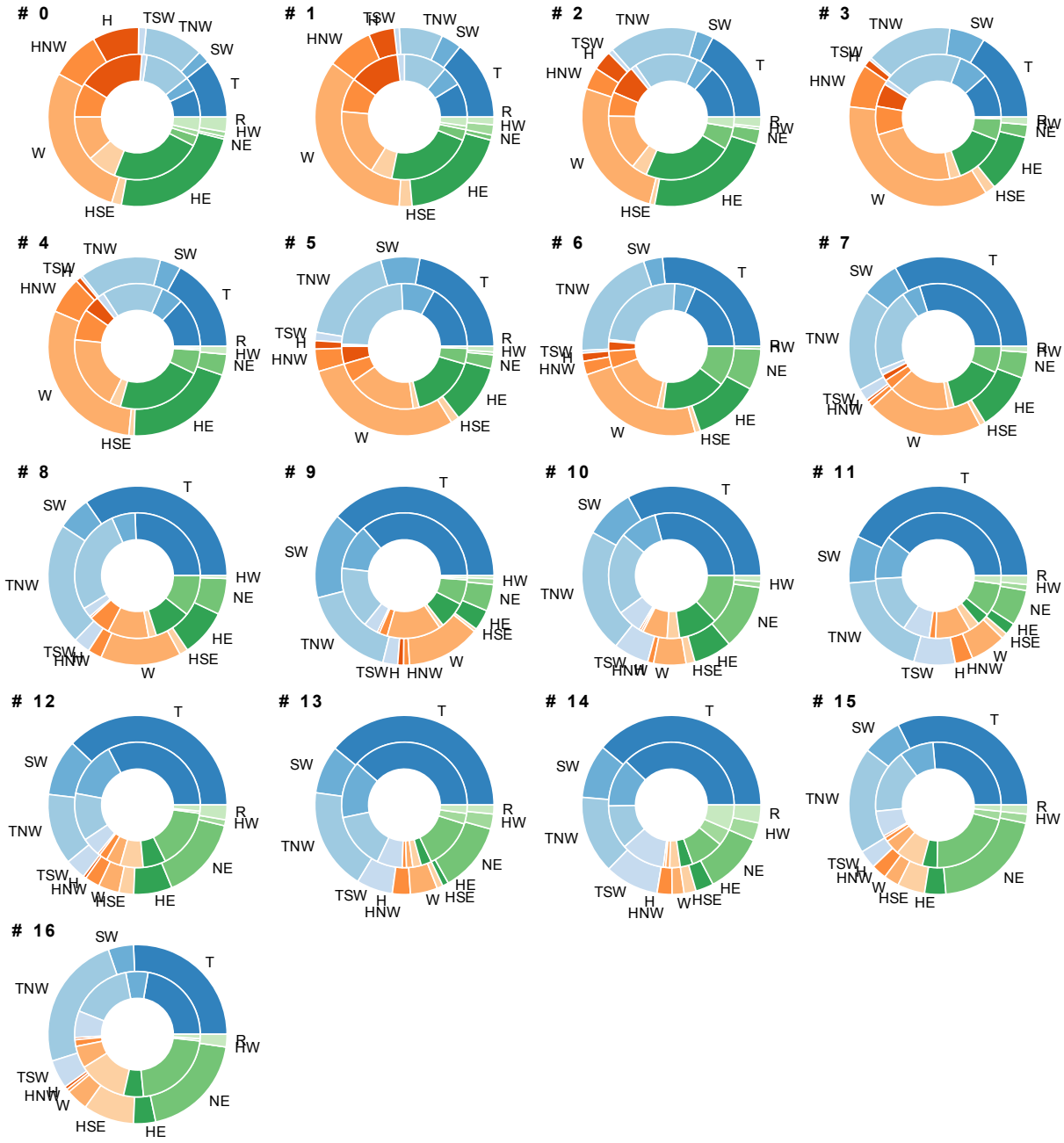

Supplementary Figure 2. Pie plots as shown in Fig. 4 but for the 10% strongest ARs according to the Max_IVT descriptor.

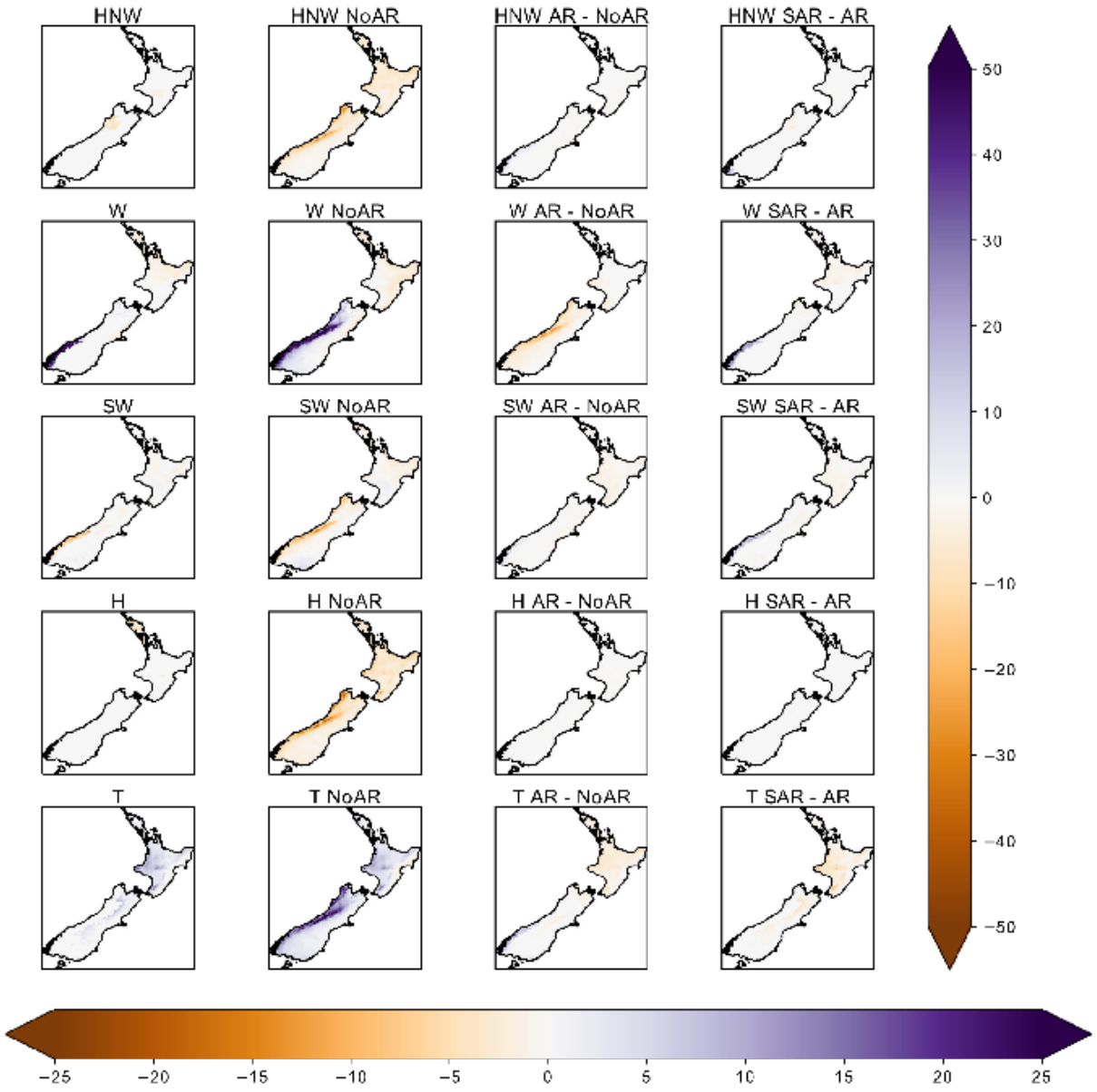

Supplementary Figure 3. (a) As Fig. 5 but for southernmost grid-point #0 (a) and northernmost grid-point #16 (b).

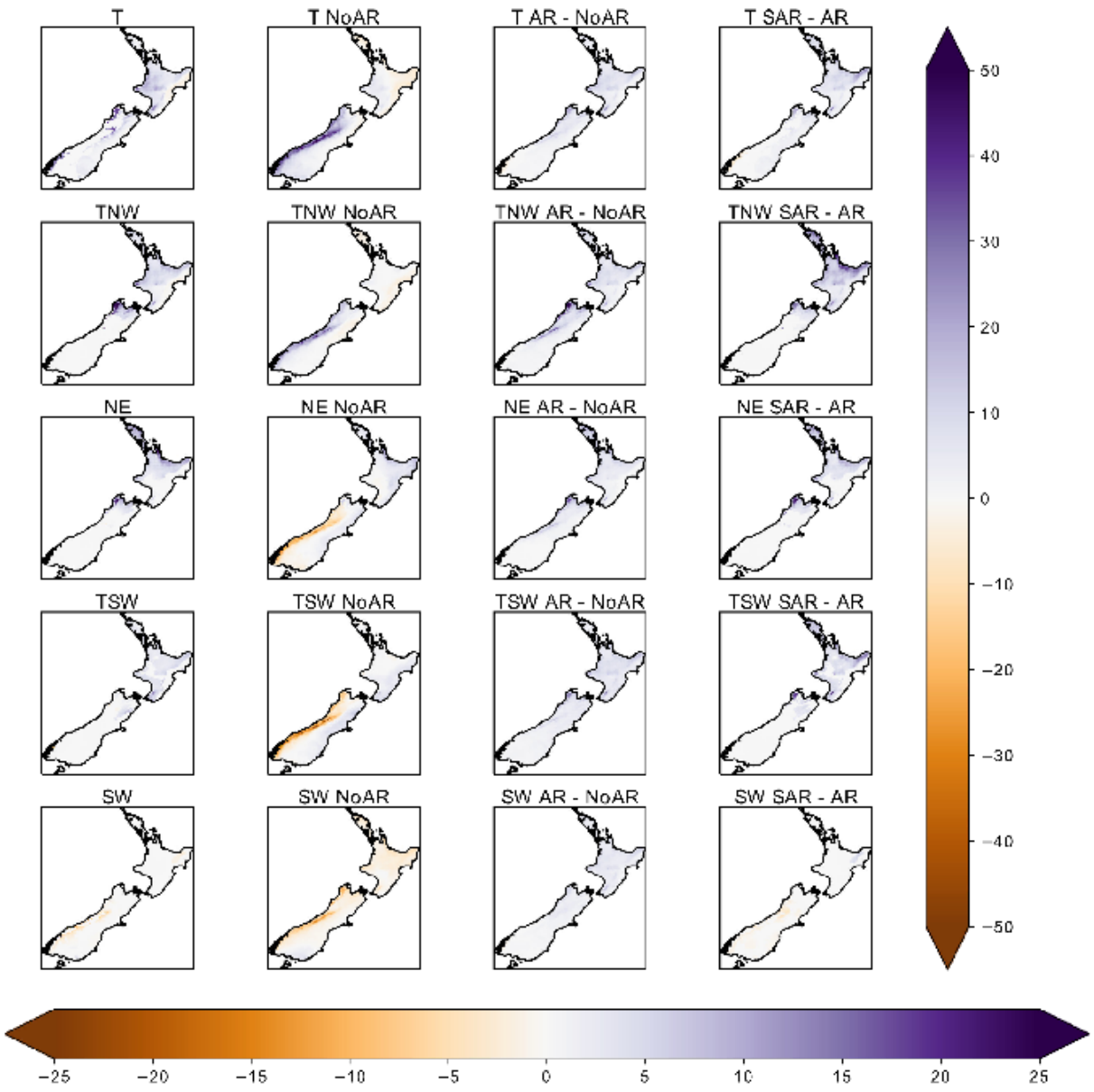

Supp. Fig. 3 (b: *continued*).

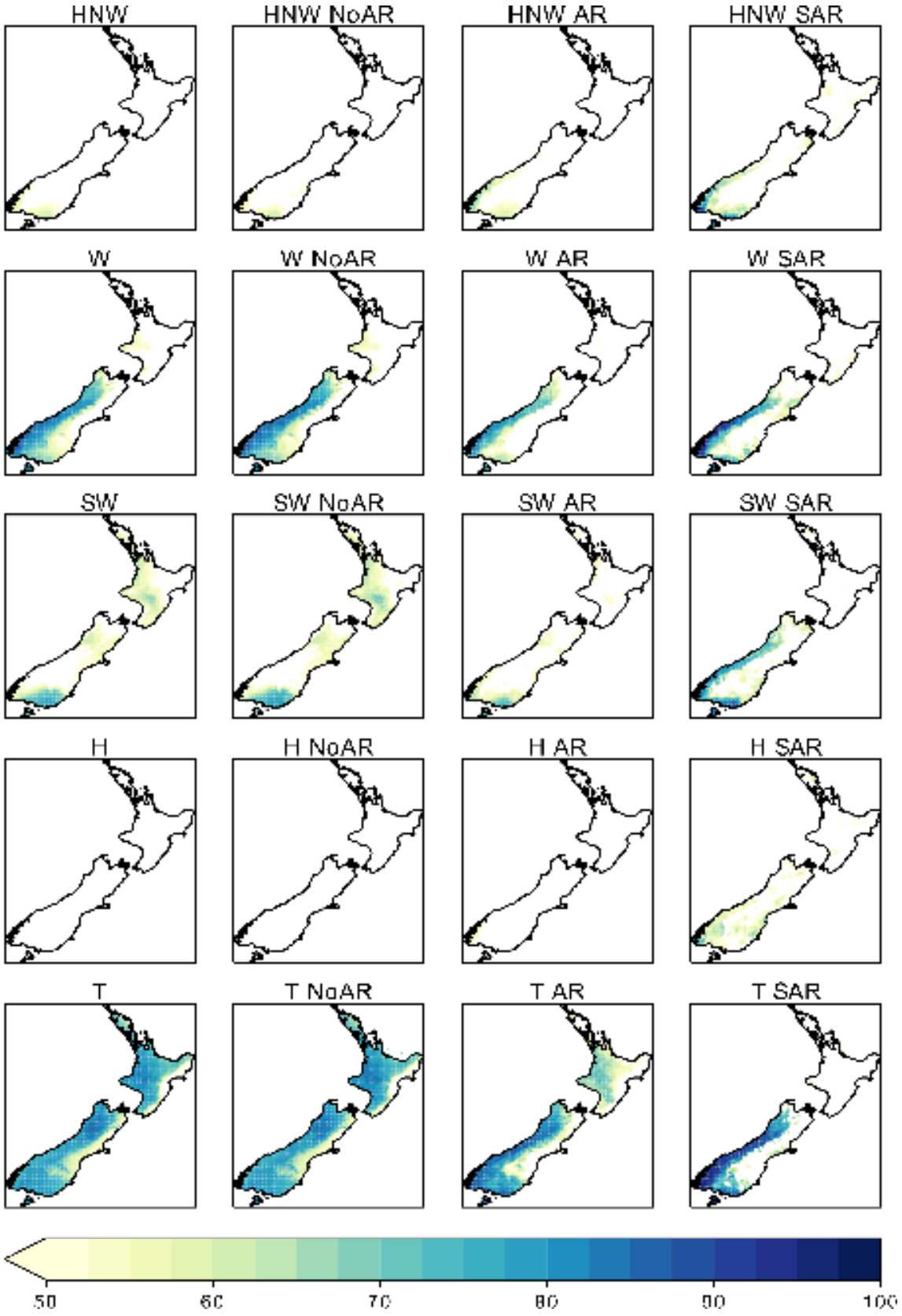

Supplementary Figure 4. (a) Rank of daily precipitation anomalies associated with the 5 most favorable regimes, for NoAR, moderate AR and strong AR days. Median of daily ranks for each WR and AR combination, for southernmost g-p #0 (a), and northernmost g-p #16 (b). ERA5 definition of WTs is used.

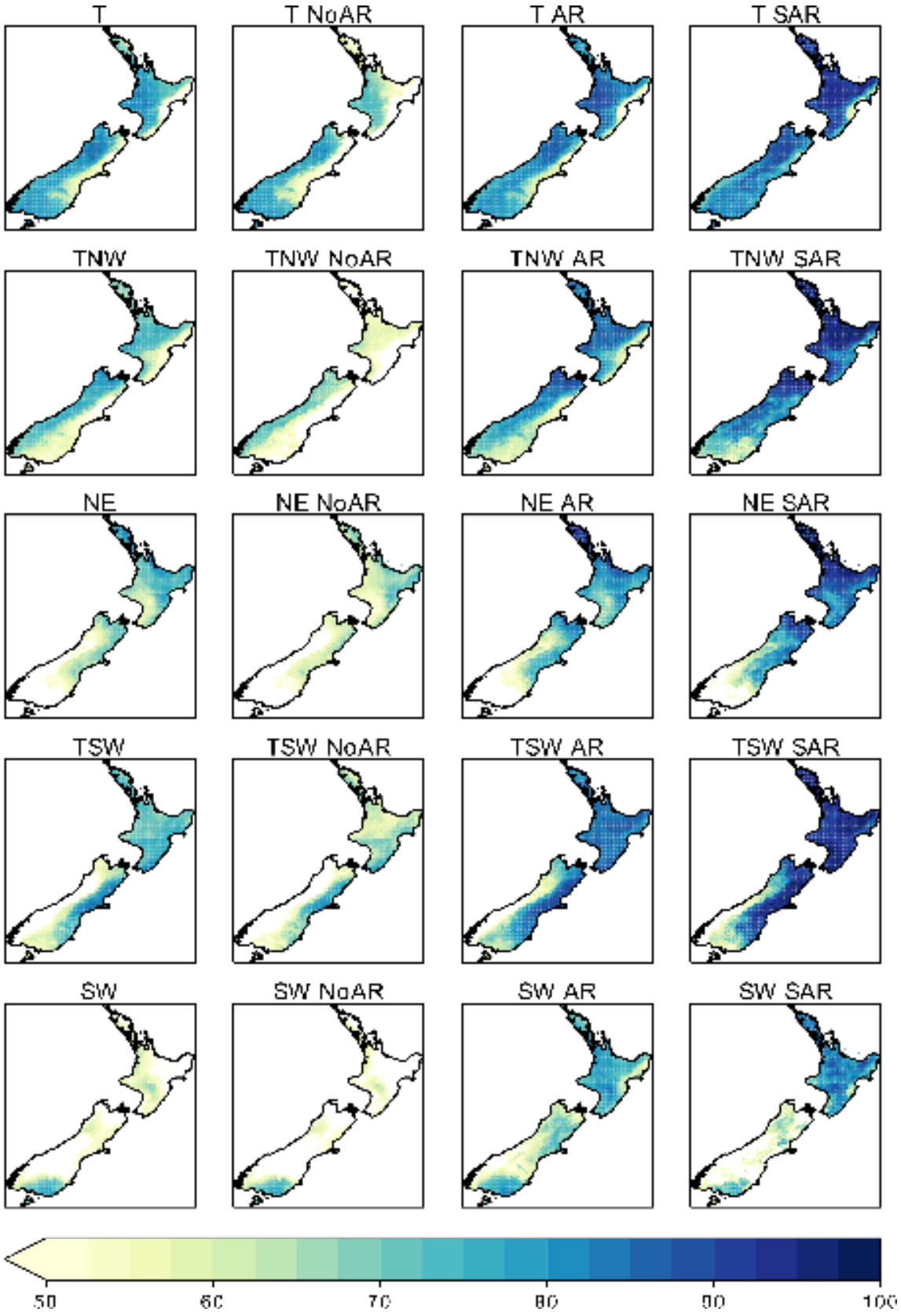

Supp. Fig. 4 (b: *continued*).

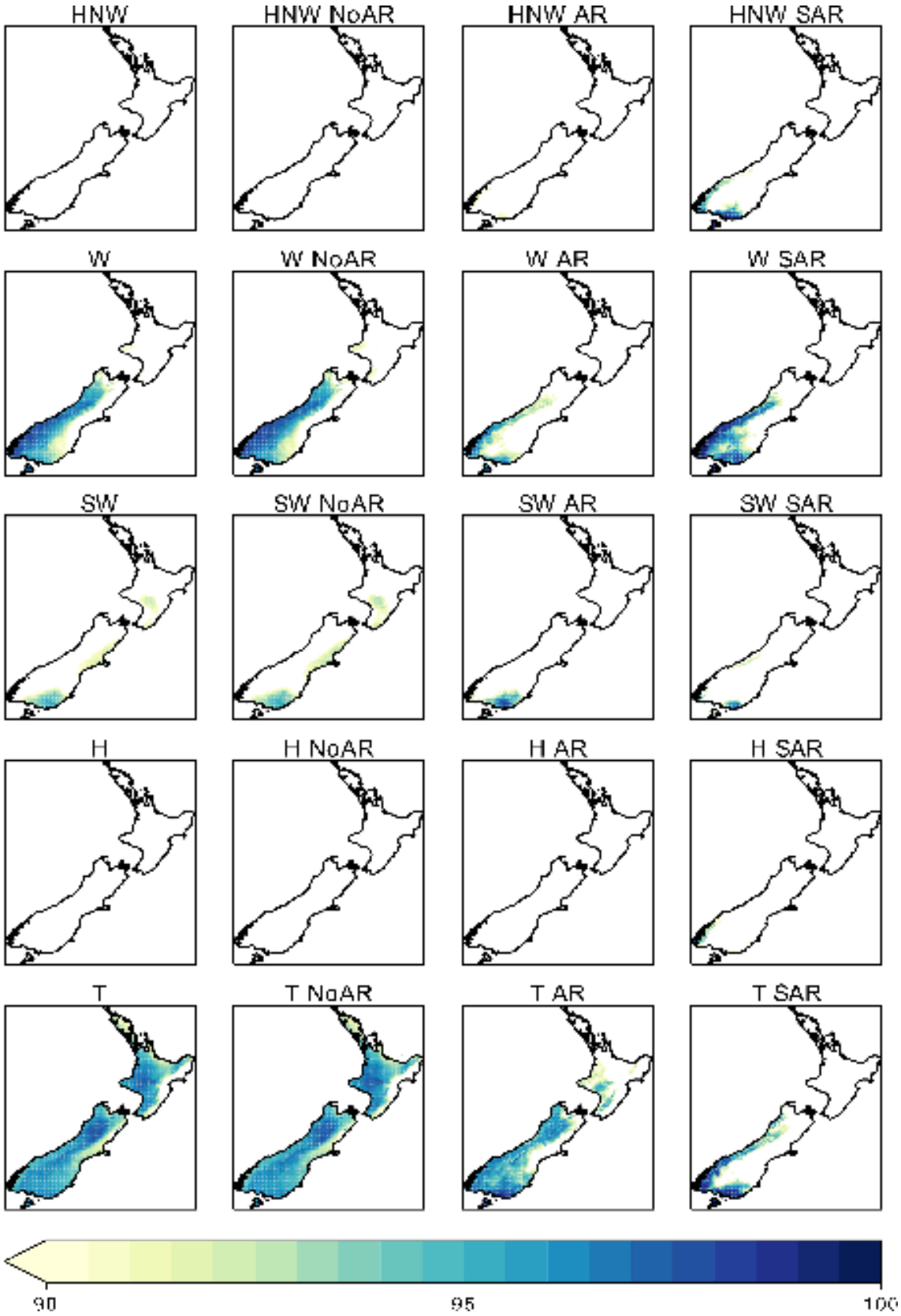

Supplementary Figure 5. (a) As Supp. Fig. 4 but for the 90th percentile of daily ranks for each WT and each AR category.

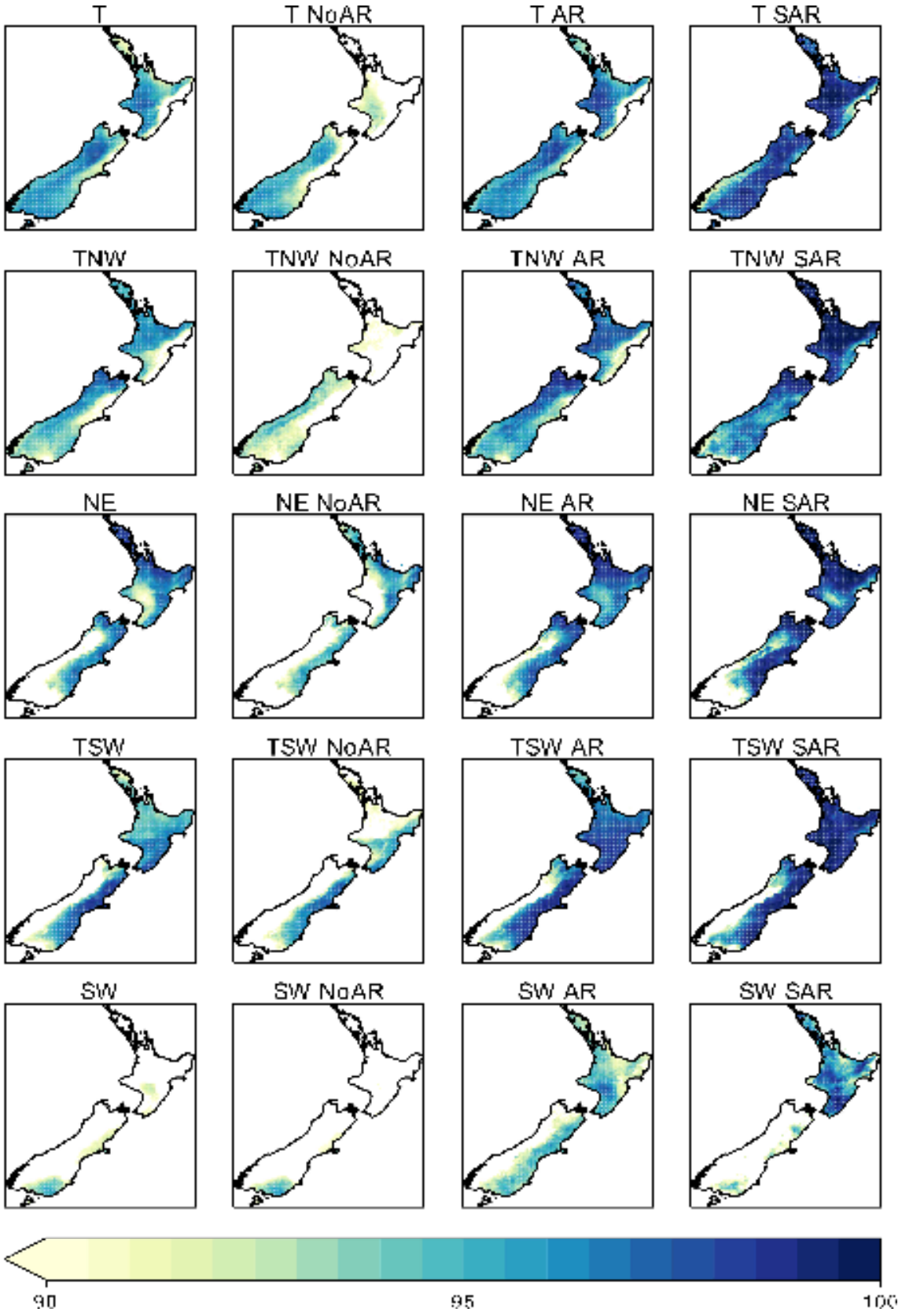

Supp. Fig. 5 (b: *continued*).

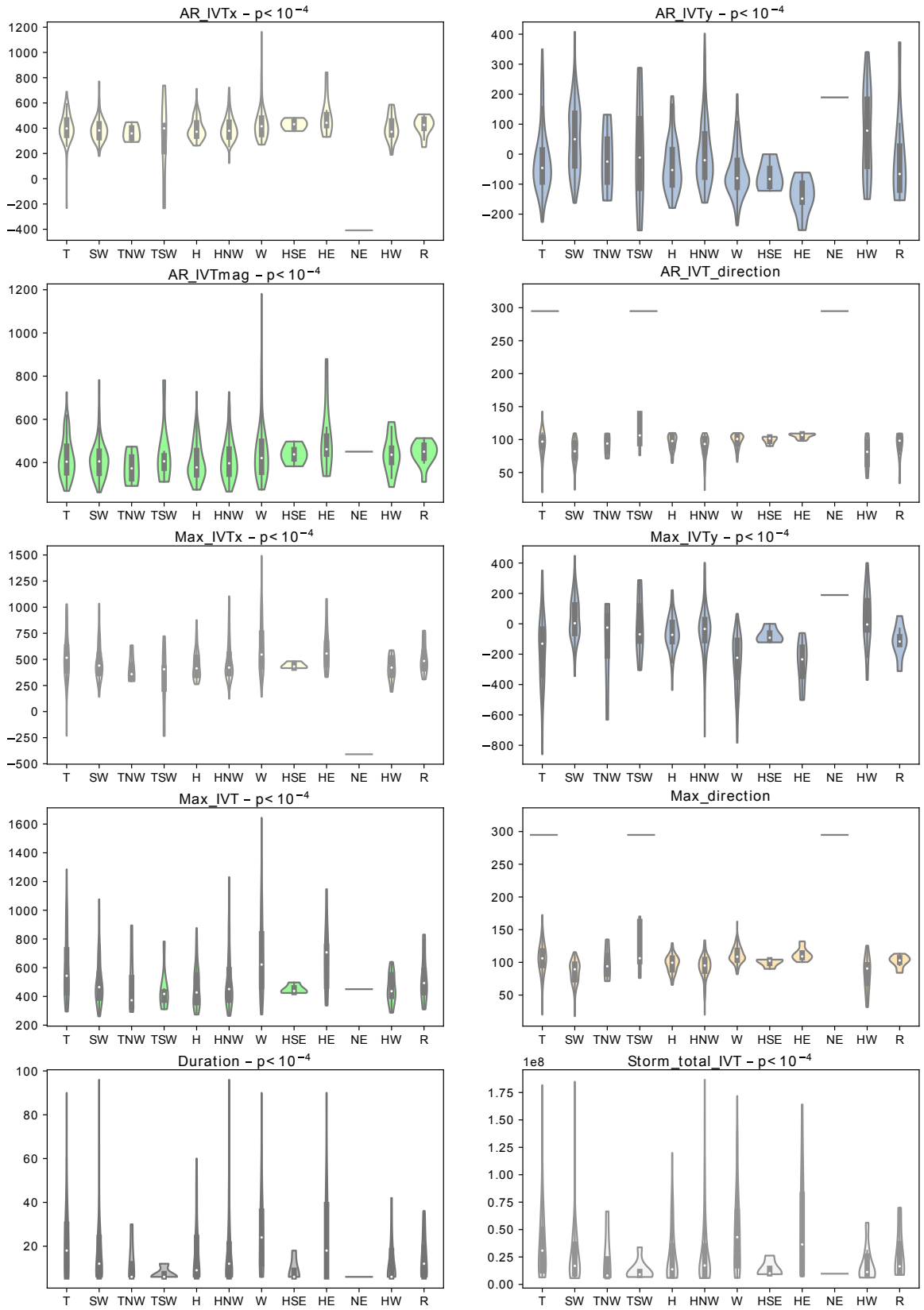

Supplementary Figure 6. (a) As Fig. 7 but for southernmost grid-point #0 (a) and northernmost grid-point #16 (b).

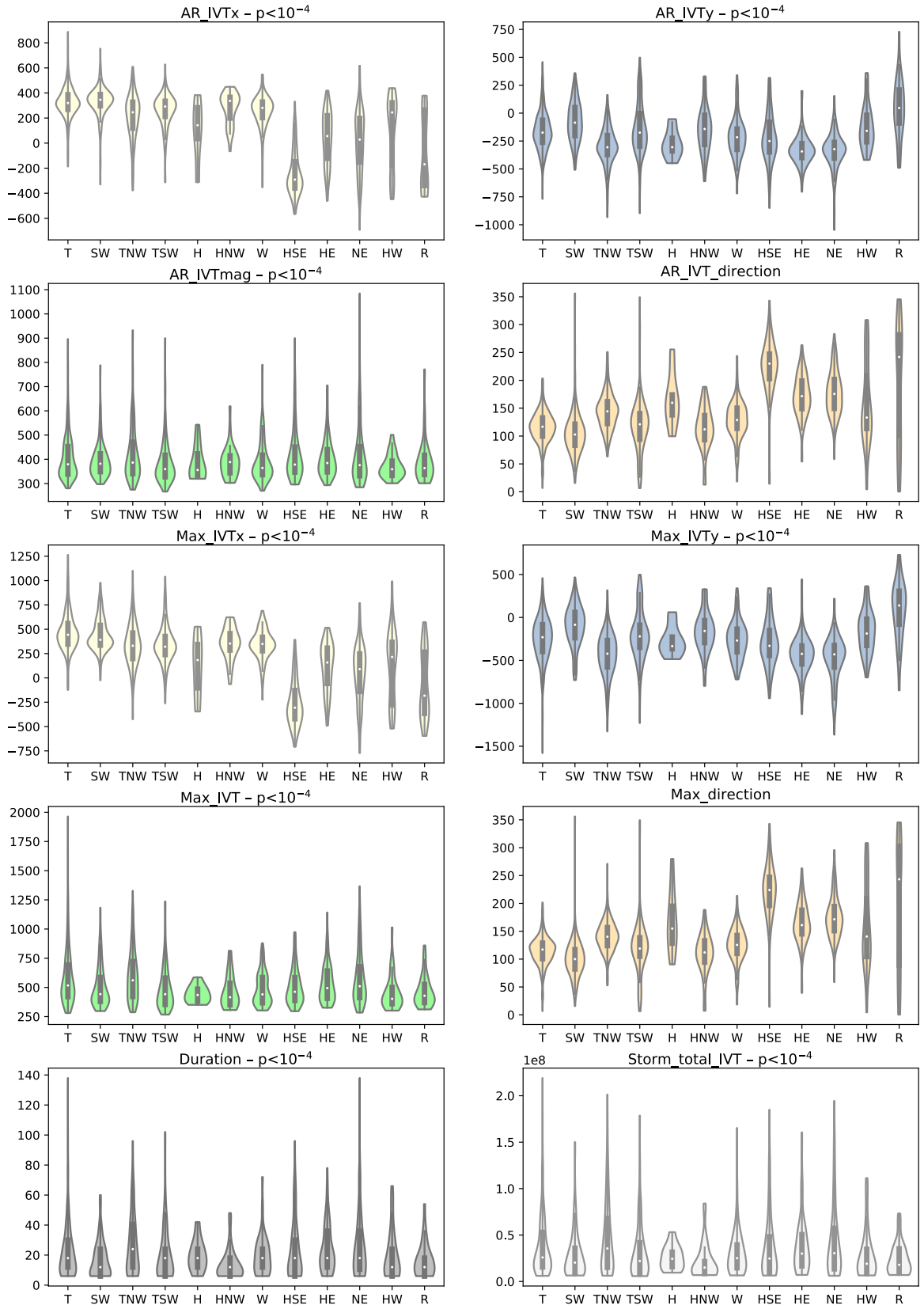

Supp. Fig. 6 (b: *continued*).

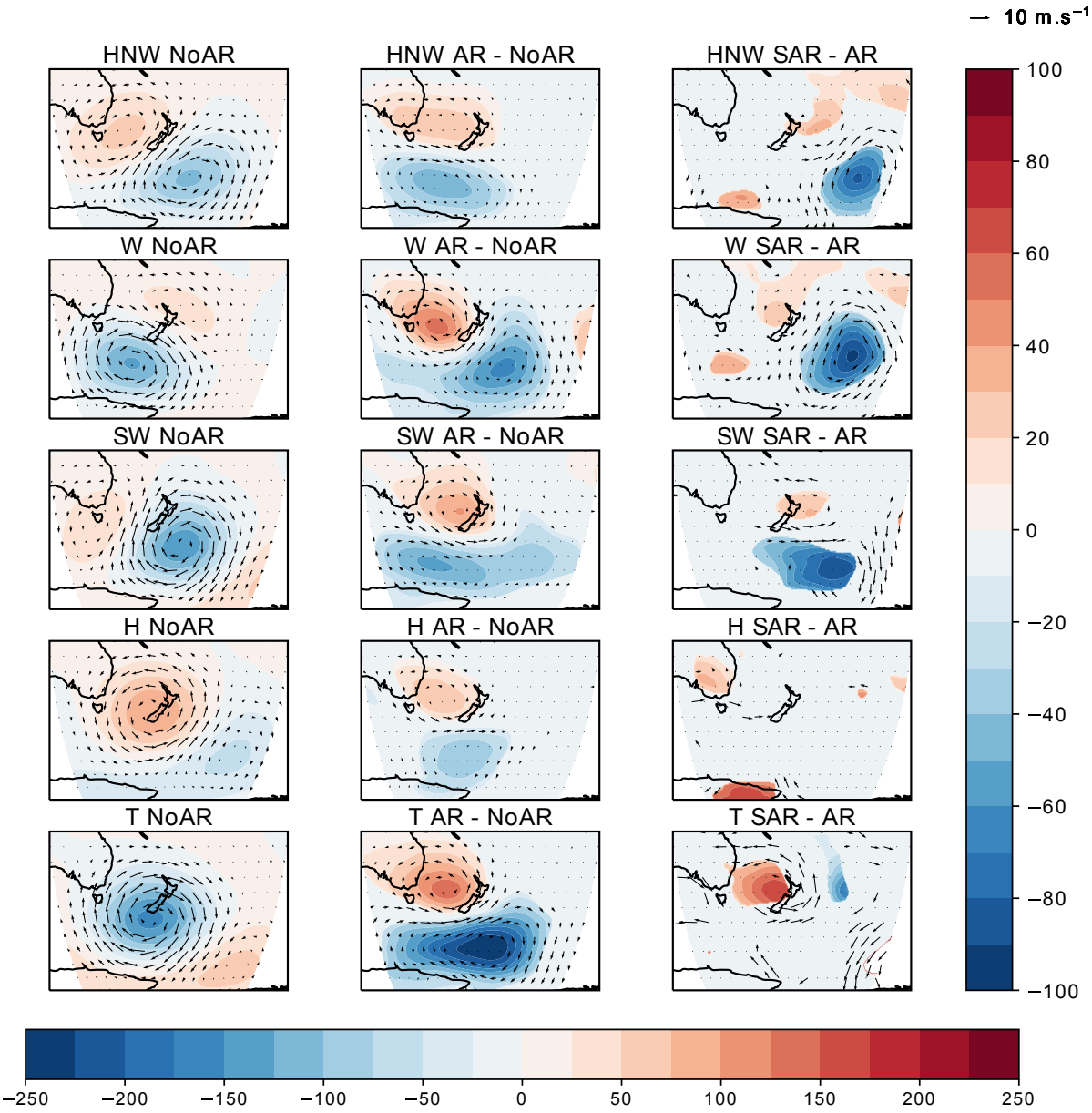

Supplementary Figure 7. (a) As Fig. 8 but for the southernmost grid-point #0.

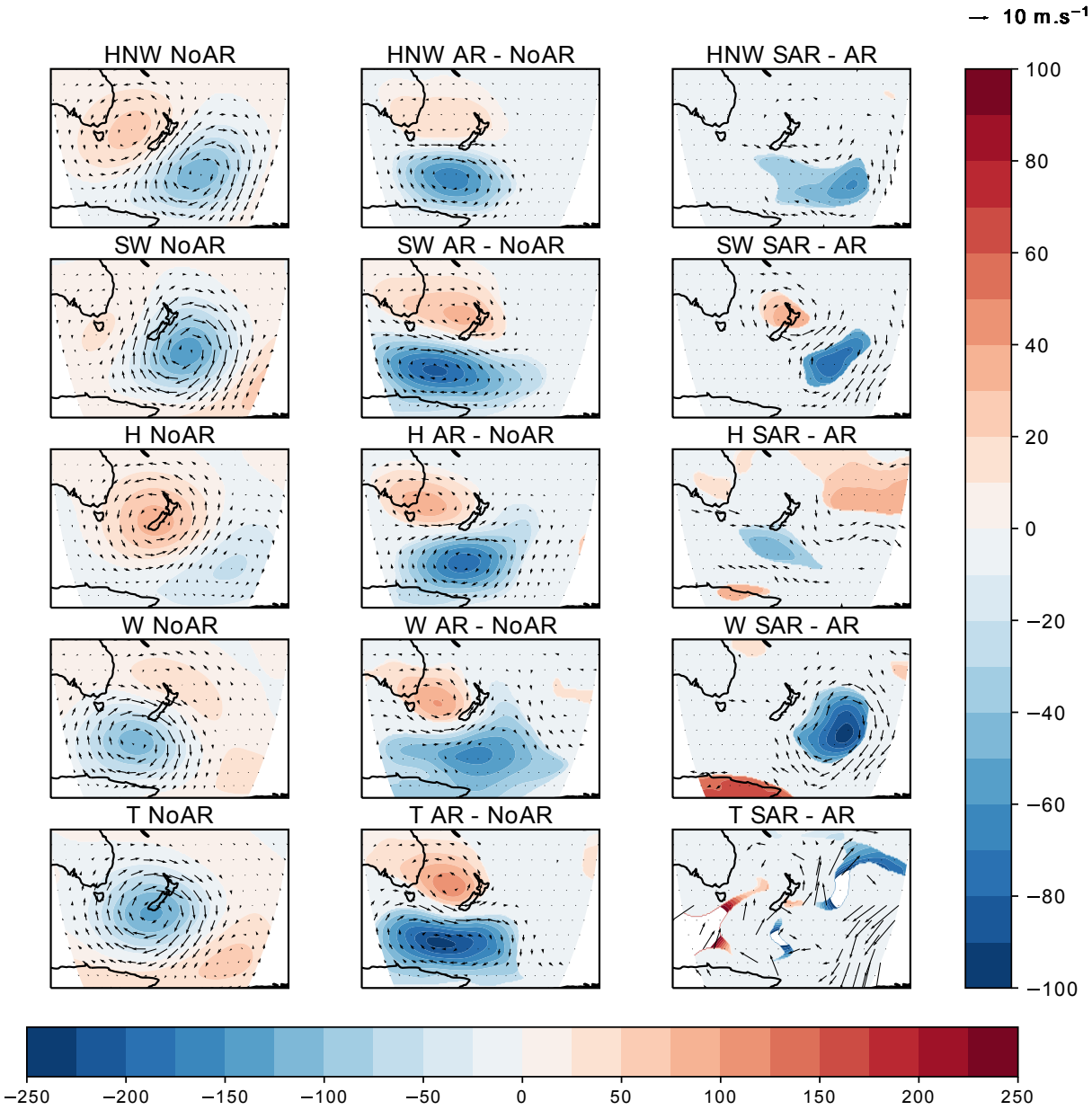

Supp. Fig. 7 (b: *continued*).

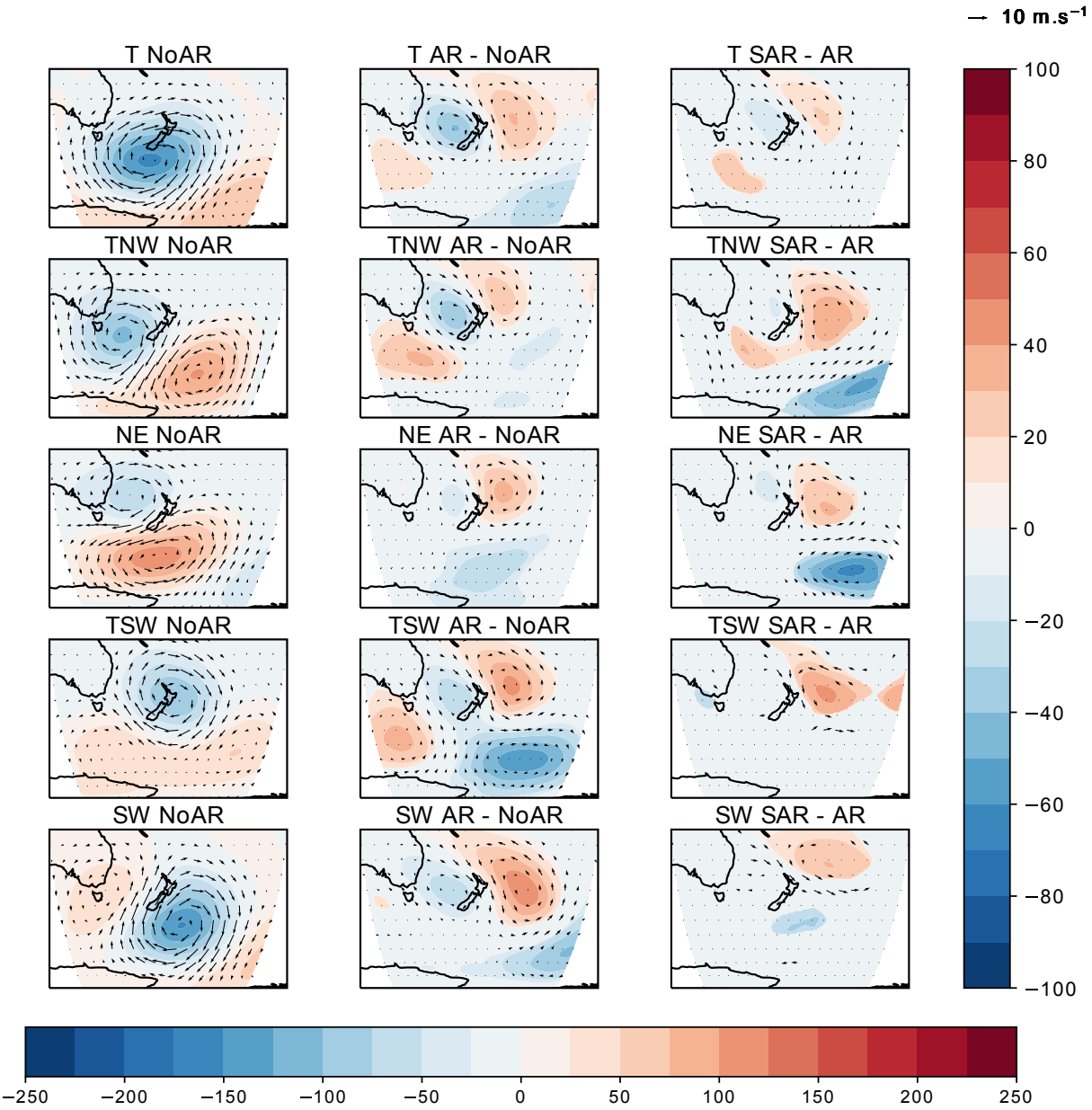

Supplementary Figure 8. (a) As Fig. 8 but for the northernmost grid-point #16.

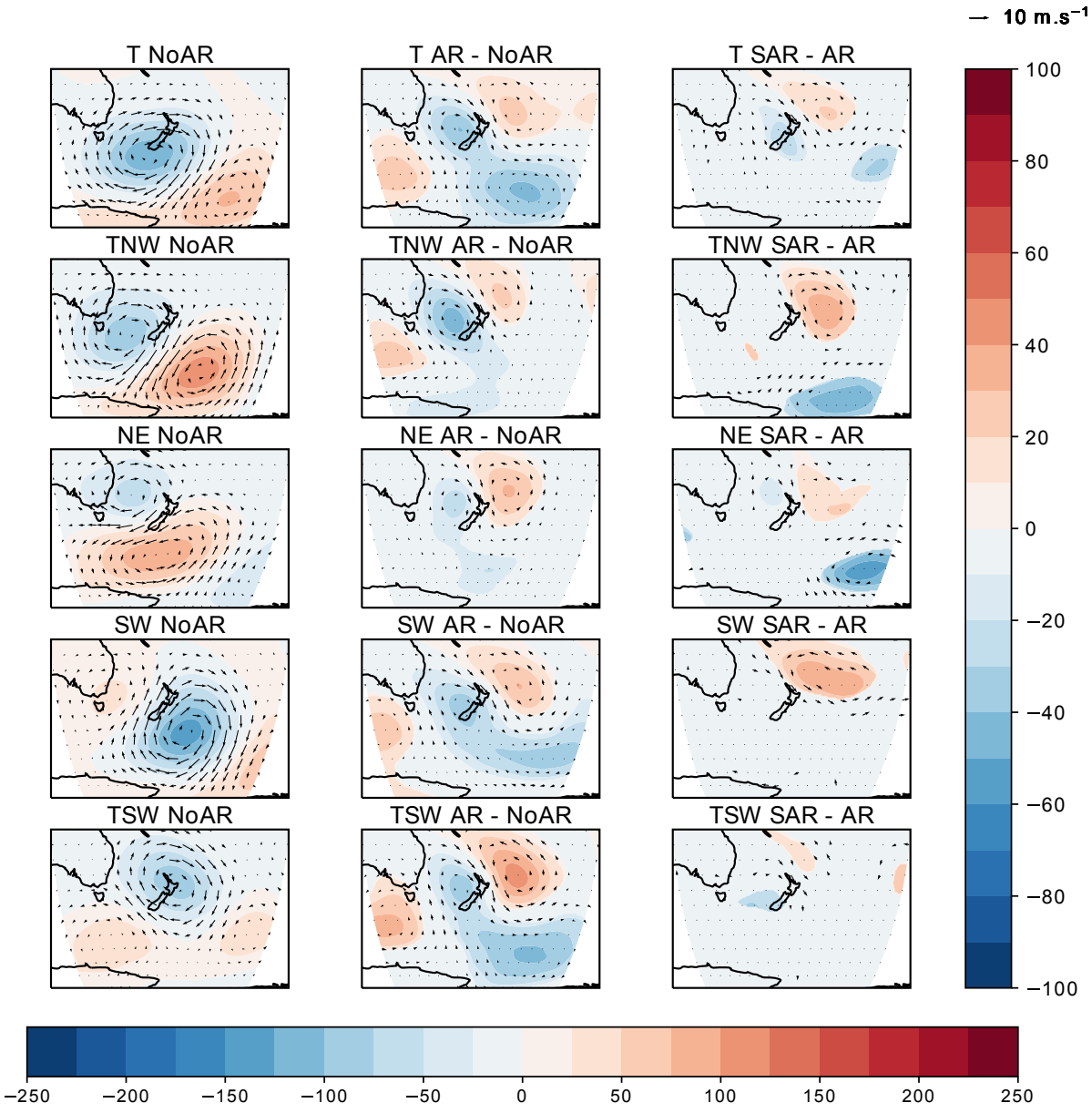

Supp. Fig. 8 (b: *continued*).

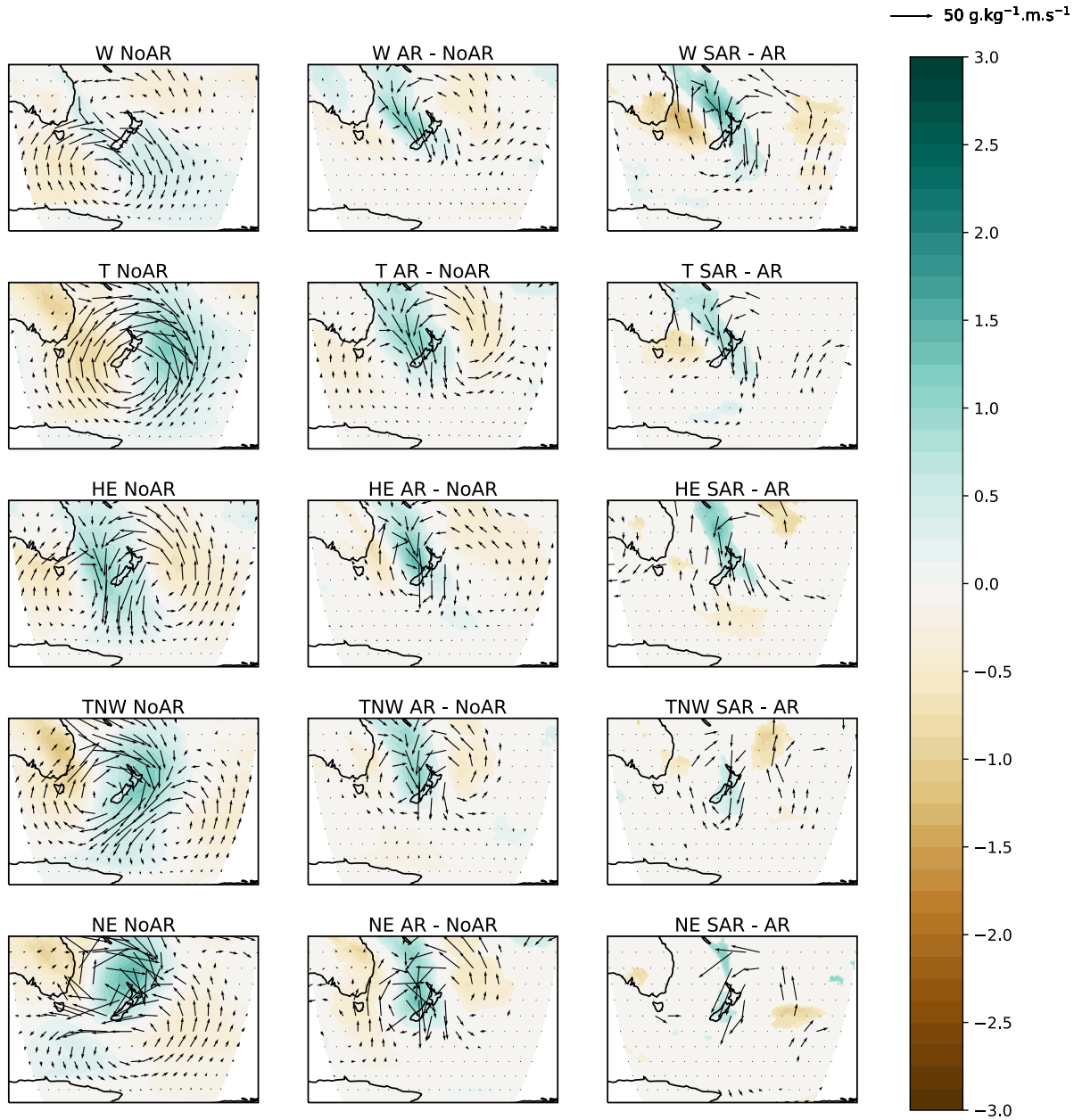

Supplementary Figure 9. (a) Differences in specific humidity and moisture fluxes between WTs associated and not associated with ARs in (a) grid-point #6 (West Coast of the South Island), (b) southernmost grid-point #0, and (c) northernmost grid-point #16, using the ERA5 redefinition of WTs. Composite mean anomalies of specific humidity at 1000hPa (colors: $g.kg^{-1}$) and 1000hPa horizontal moisture fluxes (vectors: $g.kg^{-1}.m.s^{-1}$) anomalies during the 5 most favorable WTs. In each figure: left column, most favorable WTs when not associated with ARs. Middle column: difference between NoAR and moderate AR occurrences of the same WTs. Right: difference between strong ARs (SAR: top 10% IVT) and moderate ARs. For the two first columns (lower colorbar), only significant anomalies according to one-tailed t-tests modified by Welch (95% level) are displayed. For the third column (right-hand colorbar), only significant differences according to two-tailed t-tests modified by Welch (95% level) are displayed.

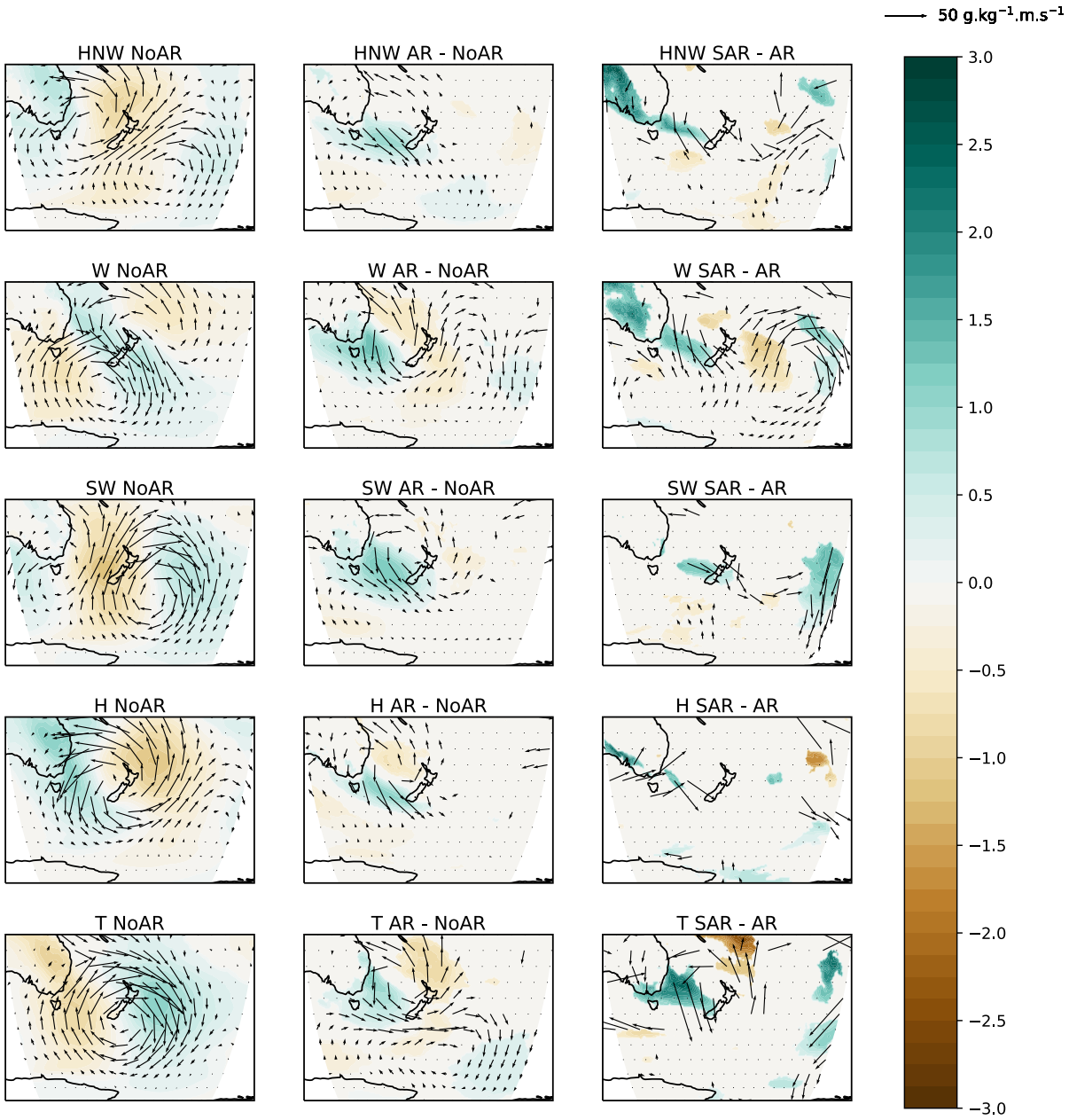

Supp. Fig. 9 (b: *continued*).

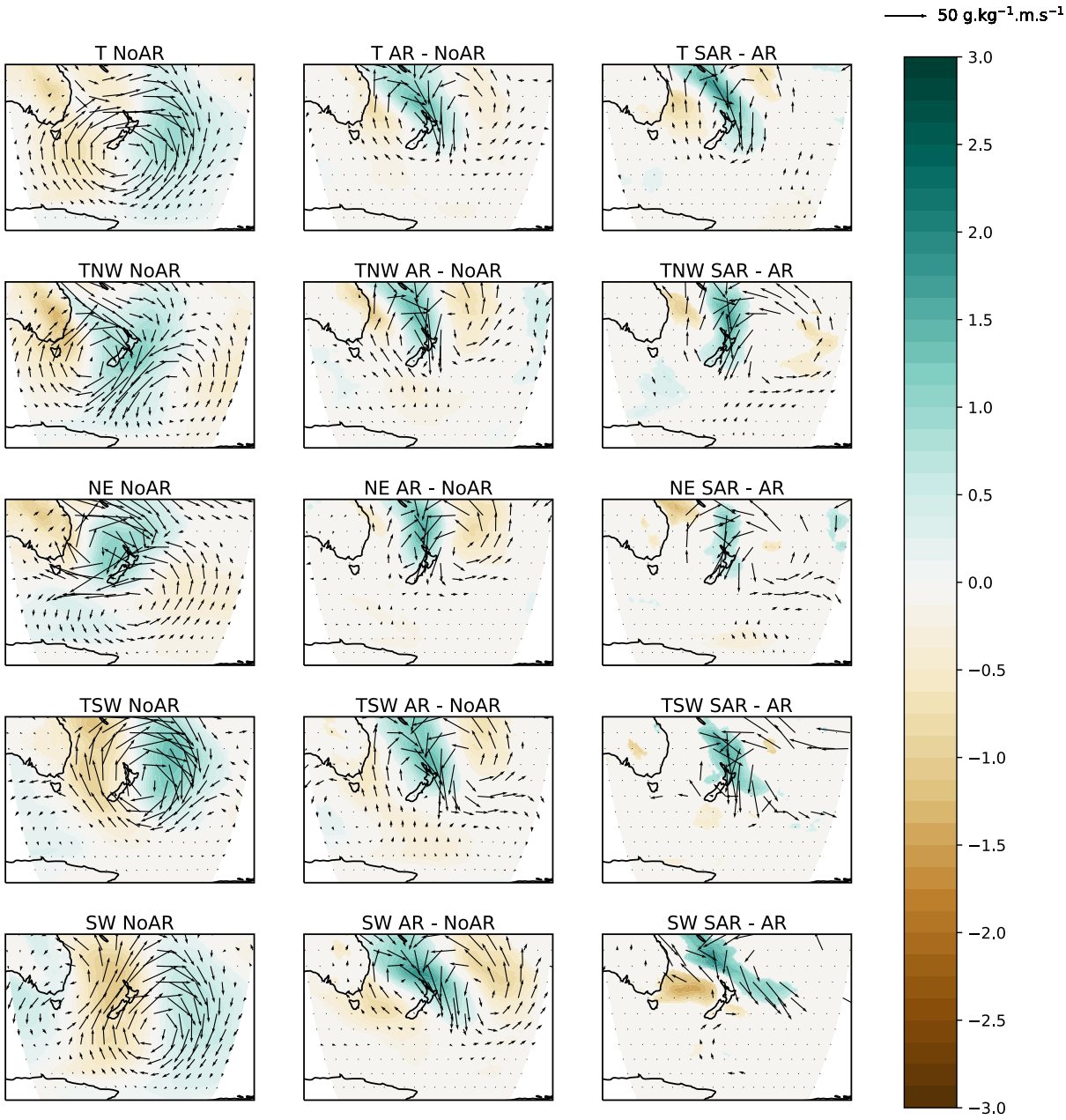

Supp. Fig. 9 (c: *continued*).

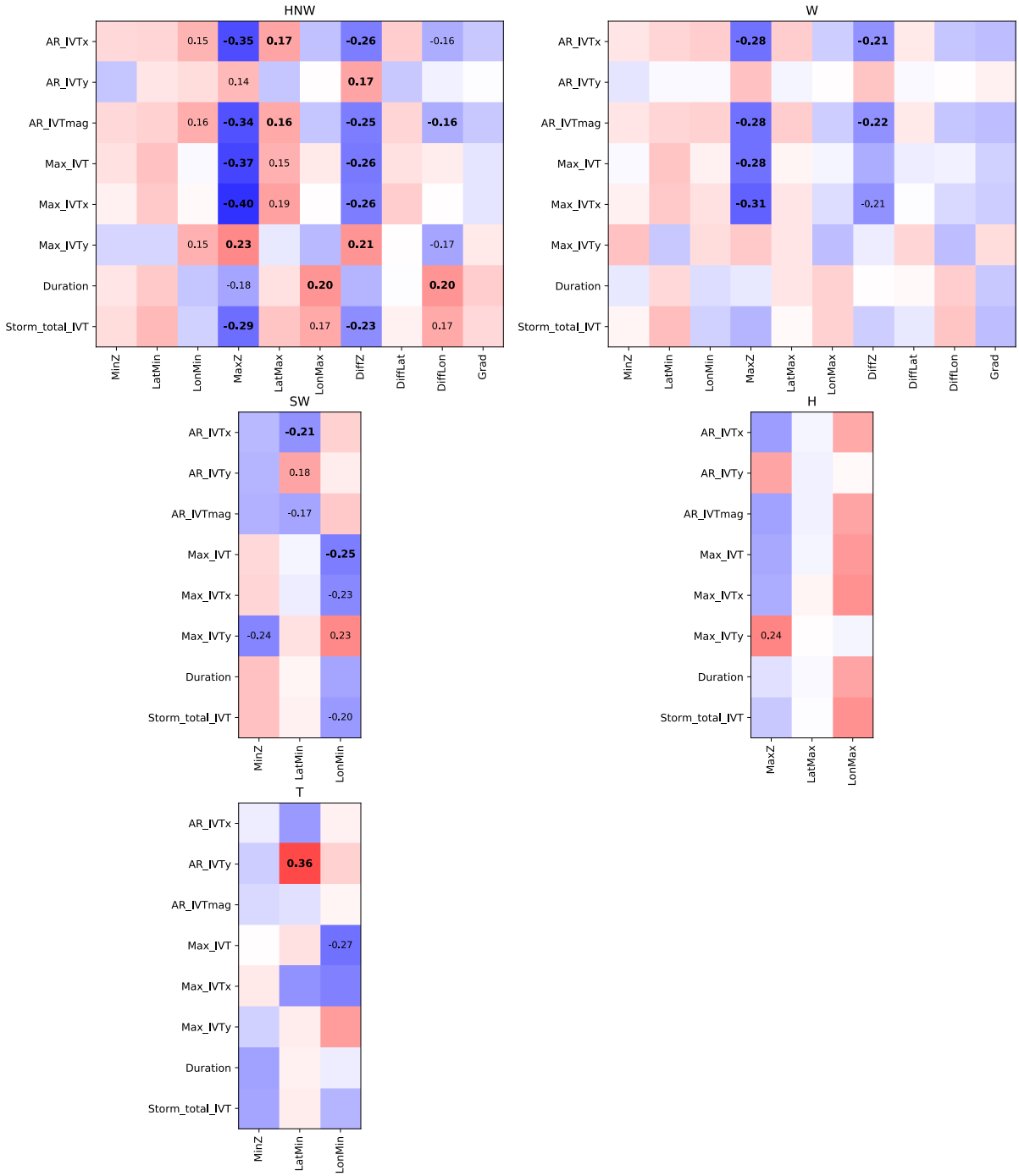

Supplementary Figure 10. (a) As Fig. 9 but for southernmost grid-point #0.

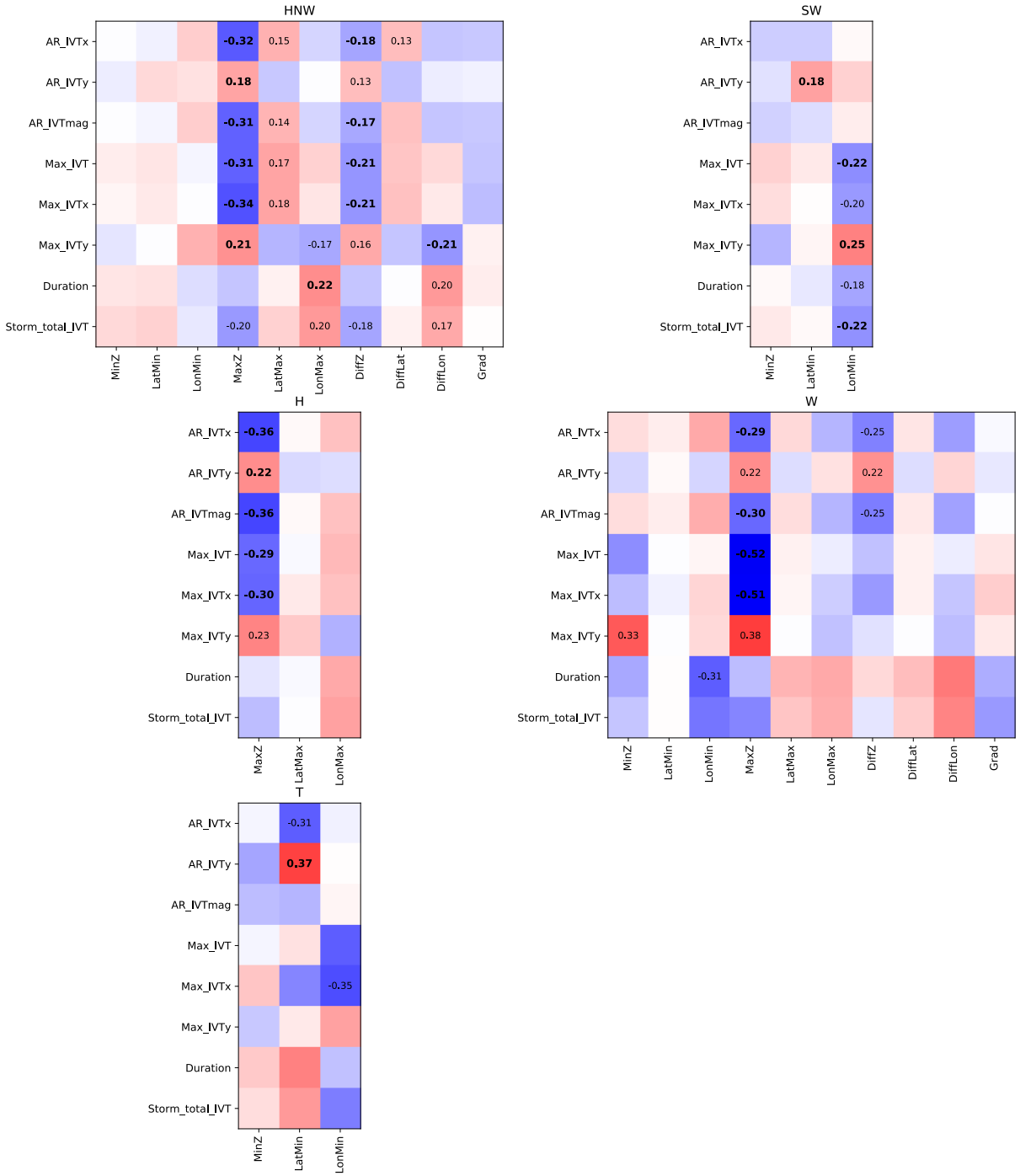

Supplementary Figure 10 (b: *continued*).

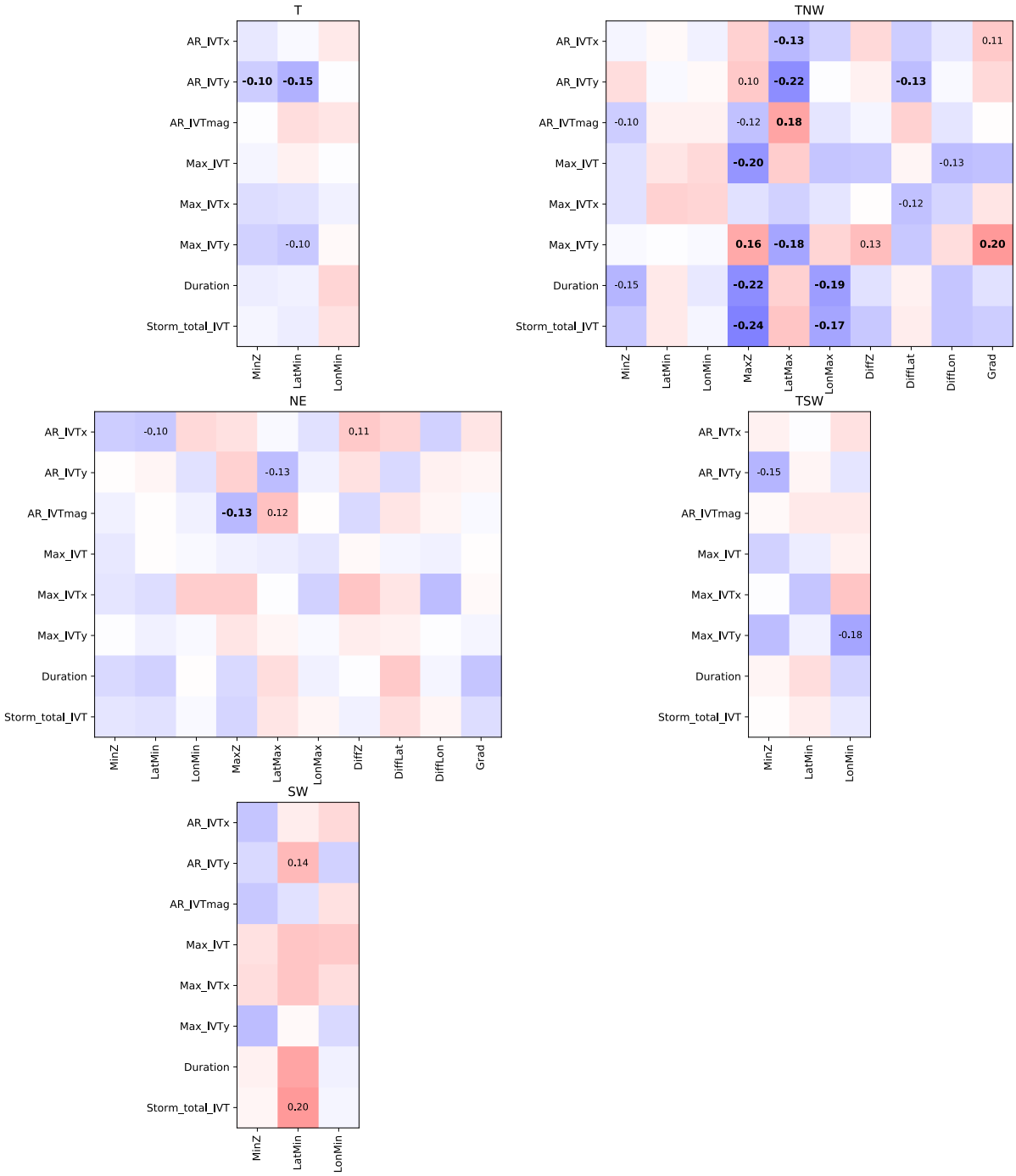

Supplementary Figure 11. (a) As Fig. 9 but for northernmost grid-point #16.

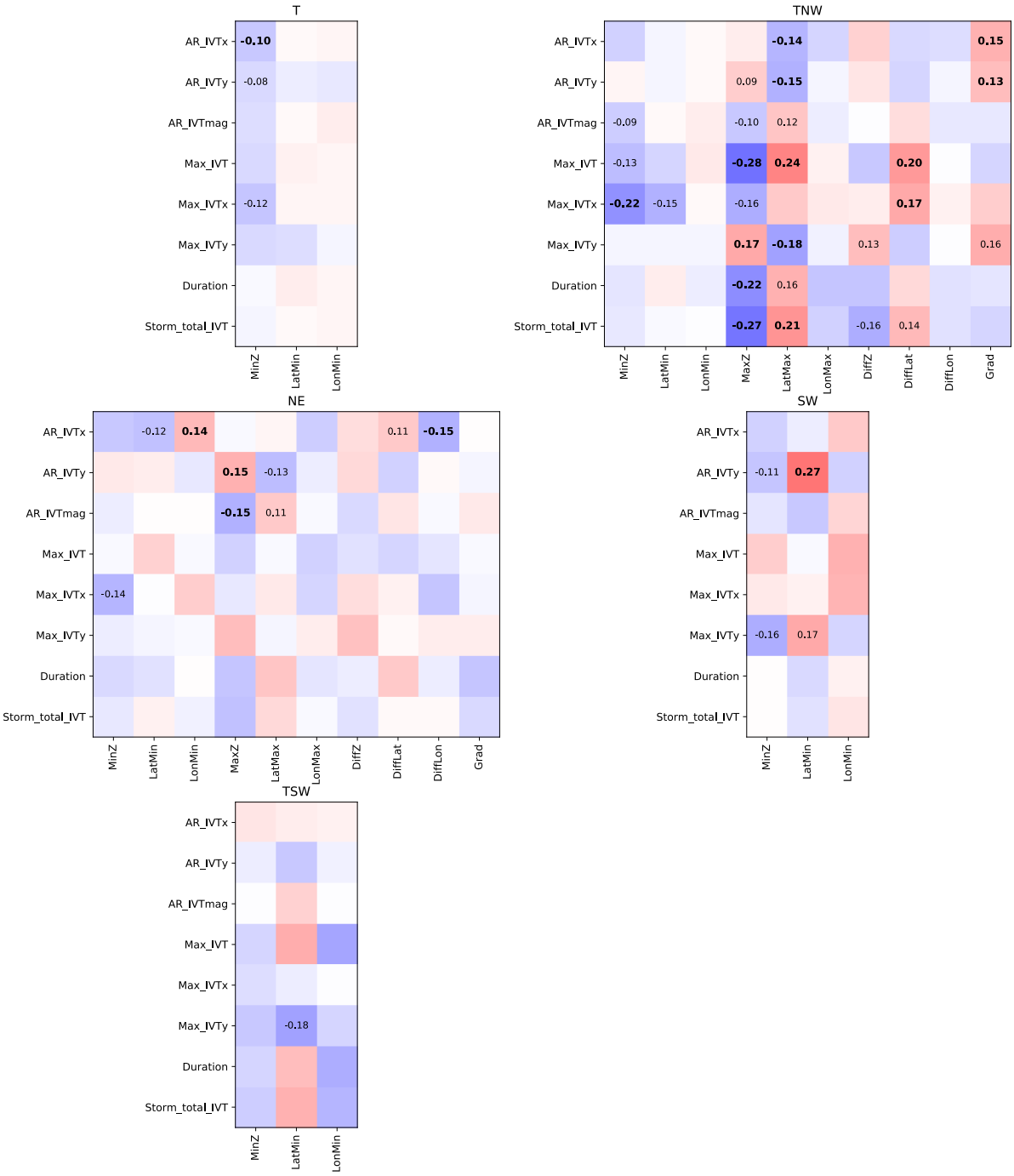

Supplementary Figure 11 (b: *continued*).